

論文 / 著書情報  
Article / Book Information

Title	Accelerating EUV lithography simulation with weakly guiding approximation and STCC formula
Authors	Hiroyoshi Tanabe, Akira Jinguji, Atsushi Takahashi
Citation	Proc. SPIE 12750, International Conference on Extreme Ultraviolet Lithography 2023, 127500D, , ,
Pub. date	2023, 11
DOI	<a href="https://doi.org/10.1117/12.2688029">https://doi.org/10.1117/12.2688029</a>
Rights	<p>(Copyright) Copyright 2023 Society of Photo Optical Instrumentation Engineers (SPIE). One print or electronic copy may be made for personal use only. Systematic reproduction and distribution, duplication of any material in this publication for a fee or for commercial purposes, and modification of the contents of the publication are prohibited.</p> <p>(Citation) Hiroyoshi Tanabe, Akira Jinguji, and Atsushi Takahashi "Accelerating EUV lithography simulation with weakly guiding approximation and STCC formula", Proc. SPIE 12750, International Conference on Extreme Ultraviolet Lithography 2023, 127500D (21 November 2023); <a href="https://doi.org/10.1117/12.2688029">https://doi.org/10.1117/12.2688029</a></p>

# PROCEEDINGS OF SPIE

[SPIDigitalLibrary.org/conference-proceedings-of-spie](https://spiedigitallibrary.org/conference-proceedings-of-spie)

## Accelerating EUV lithography simulation with weakly guiding approximation and STCC formula

Hiroyoshi Tanabe, Akira Jinguji, Atsushi Takahashi

Hiroyoshi Tanabe, Akira Jinguji, Atsushi Takahashi, "Accelerating EUV lithography simulation with weakly guiding approximation and STCC formula," Proc. SPIE 12750, International Conference on Extreme Ultraviolet Lithography 2023, 127500D (21 November 2023); doi: 10.1117/12.2688029

**SPIE.**

Event: SPIE Photomask Technology + EUV Lithography, 2023, Monterey, California, United States

# Accelerating EUV lithography simulation with weakly guiding approximation and STCC formula

Hiroyoshi Tanabe,\* Akira Jinguji and Atsushi Takahashi  
Tokyo Institute of Technology, 2-12-1 Ookayama, Meguro-ku, Tokyo 152-8550 Japan

## ABSTRACT

In our previous works, a convolutional neural network was developed which predicted diffraction amplitudes from extreme ultraviolet masks very fast. In this work, we reduce both the time for preparing the training data and the time for image intensity integration. We reduce the time for preparing the training data by applying weakly guiding approximation to 3D waveguide model. The model solves Helmholtz type coupled vector wave equations of two polarizations. The approximation decomposes the coupled vector wave equations into two scalar wave equations, reducing the computation time to solve the equations. Regarding the image intensity integration, Abbe's theory has been used in electromagnetic simulations. Transmission cross coefficient (TCC) formula is known to be faster than Abbe's theory, but TCC formula cannot be applied to source position dependent diffraction amplitudes in electromagnetic simulations. We derive source position dependent TCC formula starting from Abbe's theory to accelerate the image intensity integration.

**Keywords:** lithography simulation, neural network, EUV mask

\*tanabe.h.af@m.titech.ac.jp

## 1. INTRODUCTION

High aspect absorbers used in extreme ultraviolet (EUV) masks induce several mask 3D (M3D) effects such as critical dimension (CD) error and edge placement error.<sup>1,2</sup> It is necessary to include the M3D effects in EUV lithography simulations. M3D effects are caused by the distorted diffraction amplitude from an EUV mask. The diffraction amplitude can be calculated rigorously by using electromagnetic (EM) simulators.<sup>3-5</sup> However, the calculation is highly time consuming, especially for optical proximity correction (OPC) applications.

To speed up the EM simulations, several approximation models were proposed which decomposed a mask pattern into 2D, 1D and 0D patterns.<sup>6-8</sup> In these models, EM field of a mask pattern was calculated by superposing the EM fields of 2D, 1D and 0D patterns. These models are currently used in many EUV lithography simulators.<sup>9-11</sup> An implicit assumption of the models is that the mask pattern is large and isolated. In some models the first order cross talks between neighboring edges are included, but higher order cross talks in the rigorous domain decomposition method<sup>12</sup> are neglected. In the case of OPC masks, the pattern densities are high because the main pattern is decorated by many serifs and assist features. Also, advanced OPC mask patterns are curvilinear. It could be difficult to apply these approximation models to OPC masks.

In our previous works,<sup>13-15</sup> a convolutional neural network (CNN) was developed which predicts the diffraction amplitude very fast from an input mask pattern. Our CNN model can be applied to arbitrary mask patterns. Although CNN prediction time is very short, preparing training data by EM simulation takes a long time. In this work we apply weakly guiding approximation to 3D waveguide model,<sup>5</sup> one of the EM simulation models, which solves Helmholtz type coupled vector wave equations. By using the weakly guiding approximation, the coupled vector wave equations are decomposed to two scalar wave equations, reducing the computation time to solve the equations.

The diffraction amplitudes calculated by EM simulations depend on the source position. Hopkins' transmission mission cross coefficient (TCC) formula, which is conventionally used in optical lithography simulations, cannot handle the source position dependent diffraction amplitudes.<sup>16</sup> Therefore, in EUV lithography simulations, Abbe's theory has been used to calculate the image intensity. However, the computation time using TCC formula is much shorter than the time using Abbe's theory, because TCC can be pre-calculated before the image intensity integration. Since the diffraction amplitude in our model is described in frequency space, the model can be easily incorporated with TCC formula. In this work we

derive source position dependent TCC (STCC) formula starting from Abbe's theory to accelerate the image intensity integration.

In Sec. 2, we explain the architecture of our CNN. In Sec. 3, we apply the weakly guiding approximation to 3D waveguide model. In Sec. 4, we derive STCC formula. Sec. 5 is the summary.

## 2. CNN FOR FAST EUV SIMULATION

In this section we explain the architecture of our CNN used for fast EUV lithography simulation.<sup>13-15</sup> Figure 1 is the schematic view of the diffraction amplitudes  $A(l, m; l_s, m_s)$  from an EUV mask. We show here the vector potential  $A$ . Inside the vacuum the vector potential is converted to the electric field  $E$  by the following equation.

$$\mathbf{E} = ik\mathbf{A} - \frac{i}{k}(\mathbf{k} \cdot \mathbf{A})\mathbf{k}, \quad (1)$$

where  $\mathbf{k}$  and  $k$  represent the wave vector and the wave number, respectively. The diffraction amplitude  $A(l, m; l_s, m_s)$  is divided into the thin mask amplitude (Fourier transform of the mask pattern)  $A^{\text{FT}}(l, m)$  and the M3D amplitude  $A^{\text{3D}}(l, m; l_s, m_s)$ .

$$A(l, m; l_s, m_s) = A^{\text{FT}}(l, m) + A^{\text{3D}}(l, m; l_s, m_s). \quad (2)$$

The M3D amplitude for each diffraction order  $(l, m)$  smoothly depends on the source position  $(l_s, m_s)$  as shown in Fig. 2. We approximate the M3D amplitude by a linear function of source position as follows.

$$A_x^{\text{3D}}(l, m; l_s, m_s) \cong a_0(l, m) + a_x(l, m)(l_s + l/2) + a_y(l, m)(m_s + m/2), \quad (3)$$

where  $a_0$  is the average of the amplitude and  $a_x$  and  $a_y$  are the slopes of the amplitude in x and y directions on the source plane, respectively. We call these three numbers as M3D parameters.

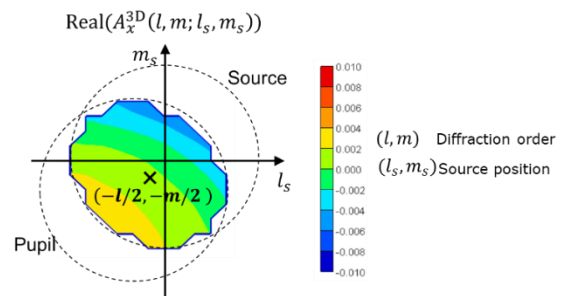
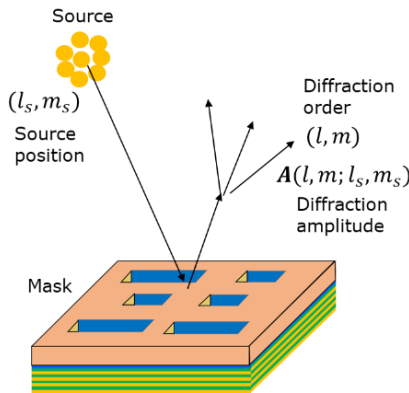


Fig. 1. Schematic view of light diffraction by an EUV mask.

Fig. 2. Source position dependence of M3D amplitude.

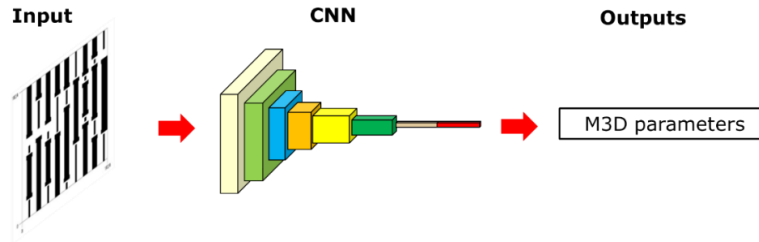


Fig. 3 CNN which connects a mask pattern and M3D parameters.

M3D parameters are determined by the mask pattern. Recently CNN is widely used as pattern recognition technique. In the previous works<sup>13-15</sup> we constructed a CNN which predicted M3D parameters from an input mask pattern (Fig. 3).

### 3. WEAKLY GUIDING APPROXIMATION OF 3D WAVEGUIDE MODEL

In the previous works<sup>14,15</sup> we used a periodic mask pattern with 256 nm X 256 nm area on the wafer. We assumed that the area was clipped from large mask data. We should not use the edges of the clipped area to avoid the influence of the neighboring mask pattern. According to Ref. 17, the optical interaction range  $R_{opt}$  is calculated by the following equation.

$$R_{opt} = \frac{1.12\lambda}{\sigma NA}, \quad (4)$$

where  $\lambda$ ,  $\sigma$ , and  $NA$  represent the wavelength, coherence factor, and numerical aperture of the scanner, respectively. The wavelength of EUV light is 13.5 nm and the numerical aperture of the current EUV scanner is 0.33. The coherence factor depends on the illumination setting.

Equation 4 can be used for conventional illumination. Here we confirm the validity of the equation for high coherent illumination, such as dipole illumination. Figure 4 shows the pitch dependence of 20 nm line CD for conventional and dipole illumination. We use a simple threshold model fixing the threshold intensity value at 40 nm pitch. CD varies depending on the pattern pitch, but it becomes stable at larger pitches where the line is isolated from the neighbor lines. The minimum pitch where CD becomes stable depends on the illumination. The minimum pitch physically corresponds to the optical interaction range. From Fig. 4, the optical interaction range for  $\sigma$  0.5 is  $\sim 100$  nm and that for dipole illumination (outer  $\sigma$  0.7, inner  $\sigma$  0.3, open angle 90 deg.) is  $\sim 150$  nm. The value for  $\sigma$  0.5 is close to  $R_{opt} \sim 90$  nm in Eq. 4. In the case of the dipole illumination the size of each monopole is  $\sim 0.3$ . From Eq. 4  $R_{opt}$  for  $\sigma$  0.3 is  $\sim 150$  nm, and it is same as the value derived from Fig. 4.

Figure 5 shows the usable mask area excluding the area influenced by the neighboring mask pattern. The mask clip size  $L$  should be larger than  $2 \times R_{opt}$  to get usable mask area. Therefore, when we use high coherent illumination the mask clip size  $L$  needs to be larger than 300 nm. In the previous works we used  $L=256$  nm, but it was not large enough for high coherent illumination. In this work we enlarge the mask clip size to 512 nm to obtain usable mask area for high coherent illumination. The usable area on the wafer is  $\sim 200$  nm X 200 nm.

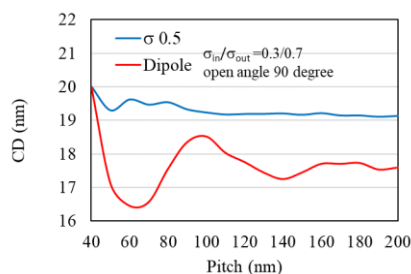


Fig. 4 Pitch dependence of 20 nm line CD.

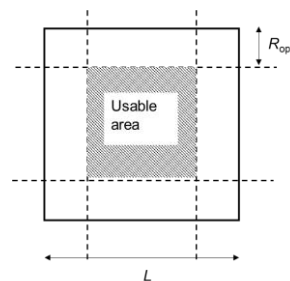


Fig. 5 Mask clip and usable area.

When we enlarge the mask clip size the computation time for EM simulations increases. We use 3D waveguide model<sup>5</sup> to solve Maxwell's equations. The calculation time for a 256 nm X 256 nm mask clip is 146 s and the time for a 512 nm X 512 nm mask clip is 2,850 s by using Core i9-10940 CPU. The model slices an EUV mask into multi layers including absorber layers and Mo/Si reflective layers. Inside each layer Maxwell's equations are reduced to the Helmholtz type coupled vector wave equations as follows.

$$\Delta A_x + k^2 \varepsilon A_x - \frac{\partial \log \varepsilon}{\partial x} \left( \frac{\partial A_x}{\partial x} + \frac{\partial A_y}{\partial y} \right) = 0, \tag{5}$$

$$\Delta A_y + k^2 \varepsilon A_y - \frac{\partial \log \varepsilon}{\partial y} \left( \frac{\partial A_x}{\partial x} + \frac{\partial A_y}{\partial y} \right) = 0, \tag{6}$$

$A_x$  and  $A_y$  are the x and y components of the vector potential.  $\varepsilon$  is the complex dielectric constant of the absorber layers or reflective layers. Inside each layer, the complex dielectric constant  $\varepsilon$  is uniform in the z direction. In this case, gauge transformation freedom allows fixing  $A_z$  to be zero.<sup>18</sup> Then  $A_z$  is omitted from the coupled vector wave equations, Eqs. 5 and 6. Inside absorber layers,  $\varepsilon$  is a function of x and y because the absorber is patterned. Inside reflective layers,  $\varepsilon$  is uniform in the x and y directions, so Eqs. 5 and 6 can be solved analytically.

Two variables,  $A_x$  and  $A_y$  correspond to two polarizations. Equation 1 indicates that the electric fields  $\mathbf{E}$  of  $A_x$  and  $A_y$  polarizations are almost parallel to x and y axis because  $k_x, k_y \ll k$  near the optical axis. Figure 6 is an example of diffraction amplitudes calculated by solving Eqs. 5 and 6 (for the details see Ref. 13). The result shows that the polarization change between the incident wave and the outgoing wave is very small. This is because the complex dielectric constant of EUV absorber is close to one. Similar phenomenon is known as “weakly guiding approximation” in optical fiber,<sup>19</sup> where two polarizations are decoupled.

We apply the weakly guiding approximation to 3D waveguide model and decompose the coupled vector wave equations. Each equation becomes a scalar wave equation as follows.

$$\Delta A_x + k^2 \varepsilon A_x - \frac{\partial \log \varepsilon}{\partial x} \frac{\partial A_x}{\partial x} = 0, \tag{7}$$

$$\Delta A_y + k^2 \varepsilon A_y - \frac{\partial \log \varepsilon}{\partial y} \frac{\partial A_y}{\partial y} = 0. \tag{8}$$

Each equation can be solved independently, and it takes 289 s for a 512 nm X 512 nm mask clip. Solving two equations take 578 s and it is ~1/5 of the time for solving original 3D waveguide model.

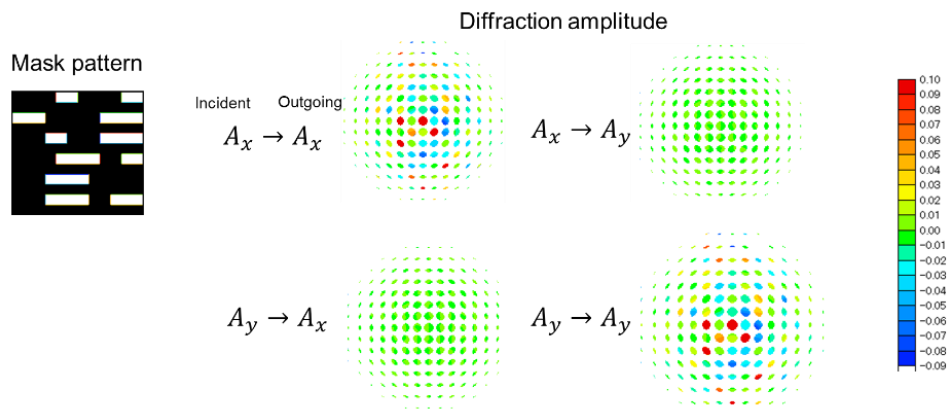


Fig. 6 Polarization dependence of the diffraction amplitudes calculated by 3D waveguide model.

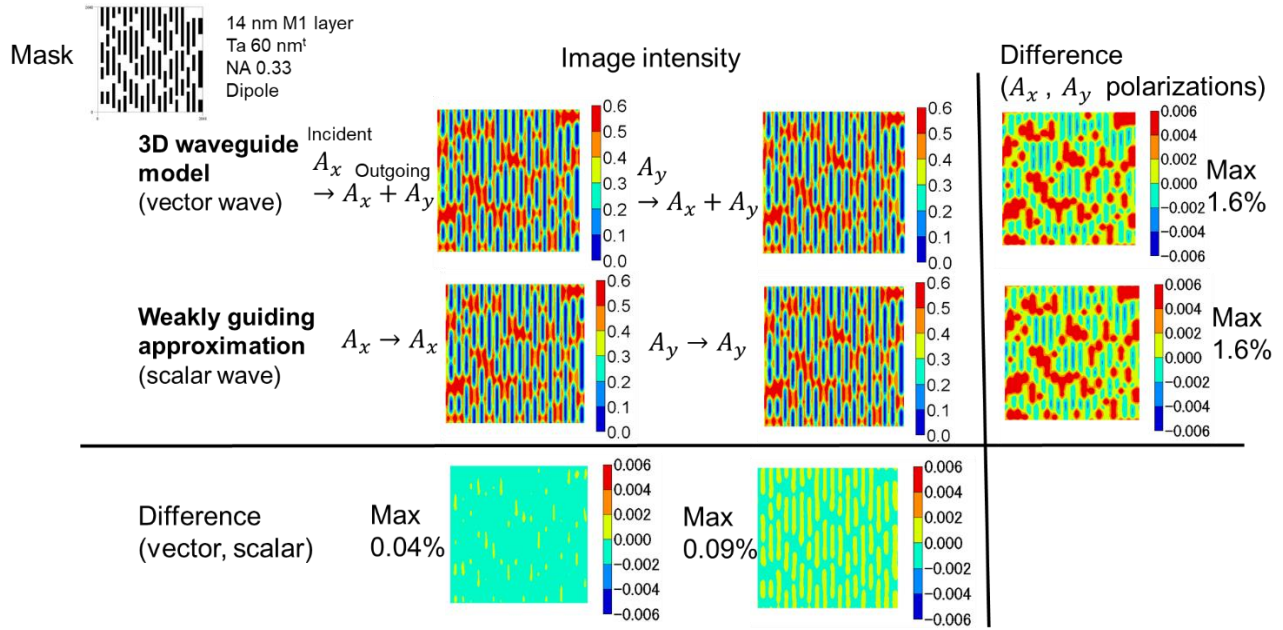


Fig. 7 Image intensities calculated by the 3D waveguide model and the weakly guiding approximation.

We confirm the accuracy of the weakly guiding approximation. Figure 7 compares the image intensities calculated by using the 3D waveguide model and the weakly guiding approximation.

The difference between the 3D waveguide model and the weakly guiding approximation is very small. Polarization changes due to the EUV mask are negligible. However, there is small difference between  $A_x$  and  $A_y$  polarizations. It is expected that the difference becomes larger for high NA scanners. Note that the result here shows the polarization effect on the mask. We did not include the polarization effect at the exit pupil of the projection optics, which is significant in high NA optics.

#### 4. SOURCE POSITION DEPENDENT TCC (STCC) FORMULA

The electric field  $E$  is calculated from the vector potential  $A$  as shown in Eq. 1. The image intensity  $I$  on the wafer is calculated by using Abbe's theory as follows.

$$I(x) = \iint S(s) \left| \iint E(k; s) P(k + s) e^{ik \cdot x} dk \right|^2 ds, \quad (9)$$

where  $S$  is the effective source and  $P$  is the pupil function of the projection optics.  $P$  is a matrix for high NA optics,<sup>20</sup> but we assume here as a scalar function. According to Eq. 3 the vector potential is approximated by a linear function of the source position  $(s_x, s_y) = 2\pi/L (l_s, m_s)$ . The electric field is also approximated by a linear function of the source position as follows.

$$I(x) \cong \iint S(s) \left| \iint \left( E(k) + \partial_{s_x} E(k)(s_x + k_x/2) + \partial_{s_y} E(k)(s_y + k_y/2) \right) P(k + s) e^{ik \cdot x} dk \right|^2 ds. \quad (10)$$

In optical lithography simulation the diffraction amplitude is Fourier transform of a mask pattern, and it does not depend on the source position. Hopkins' TCC formula<sup>16</sup> can be derived by interchanging the order of the integrals in Abbe's theory. We apply the same procedure to EUV lithography simulation. STCC formula which includes the source position dependence of the diffraction amplitudes is derived by interchanging the order of integrals in Eq. 10 as follows.



$$\begin{aligned}
I(x) \cong & \iint TCC(\mathbf{k}; \mathbf{k}') \mathbf{E}(\mathbf{k}) \cdot \mathbf{E}(\mathbf{k}')^* e^{i(\mathbf{k}-\mathbf{k}') \cdot \mathbf{x}} d\mathbf{k}d\mathbf{k}' \\
& + 2\text{Re} \left\{ \iint TCC(\mathbf{k}; \mathbf{k}') \mathbf{E}(\mathbf{k}) \cdot \left( \partial_{s_x} \mathbf{E}(\mathbf{k}') k'_x/2 + \partial_{s_y} \mathbf{E}(\mathbf{k}') k'_y/2 \right)^* e^{i(\mathbf{k}-\mathbf{k}') \cdot \mathbf{x}} d\mathbf{k}d\mathbf{k}' \right\} \\
& + 2\text{Re} \left\{ \iint TCC_x(\mathbf{k}; \mathbf{k}') \mathbf{E}(\mathbf{k}) \cdot \partial_{s_x} \mathbf{E}(\mathbf{k}')^* e^{i(\mathbf{k}-\mathbf{k}') \cdot \mathbf{x}} d\mathbf{k}d\mathbf{k}' \right\} \\
& + 2\text{Re} \left\{ \iint TCC_y(\mathbf{k}; \mathbf{k}') \mathbf{E}(\mathbf{k}) \cdot \partial_{s_y} \mathbf{E}(\mathbf{k}')^* e^{i(\mathbf{k}-\mathbf{k}') \cdot \mathbf{x}} d\mathbf{k}d\mathbf{k}' \right\}, \tag{11}
\end{aligned}$$

where  $TCC$ ,  $TCC_x$  and  $TCC_y$  are defined by the following equations.

$$TCC(\mathbf{k}; \mathbf{k}') = \iint S(s) P(\mathbf{k} + s) P^*(\mathbf{k}' + s) ds, \tag{12}$$

$$TCC_x(\mathbf{k}; \mathbf{k}') = \iint s_x S(s) P(\mathbf{k} + s) P^*(\mathbf{k}' + s) ds, \tag{13}$$

$$TCC_y(\mathbf{k}; \mathbf{k}') = \iint s_y S(s) P(\mathbf{k} + s) P^*(\mathbf{k}' + s) ds. \tag{14}$$

Sum of coherent systems (SOCS) model<sup>21</sup> is conventionally used in optical simulations to speed up the image intensity integration. SOCS model decomposes TCC into eigen functions and sums up only small number of the eigen modes to calculate the image intensity. SOCS model can also be applied to  $TCC_x$  and  $TCC_y$  because they are Hermitian matrices. Then, three TCCs are written as

$$TCC(\mathbf{k}; \mathbf{k}') = \sum_n \alpha_n \varphi_n(\mathbf{k}) \varphi_n^*(\mathbf{k}'), \tag{15}$$

$$TCC_x(\mathbf{k}; \mathbf{k}') = \sum_n \beta_n \phi_n(\mathbf{k}) \phi_n^*(\mathbf{k}'), \tag{16}$$

$$TCC_y(\mathbf{k}; \mathbf{k}') = \sum_n \gamma_n \psi_n(\mathbf{k}) \psi_n^*(\mathbf{k}'). \tag{17}$$

where  $\alpha_n, \beta_n, \gamma_n$  are eigen values and  $\varphi_n, \phi_n, \psi_n$  are eigen functions. These eigen values are real numbers.

Figure 8 compares the image intensities calculated by Abbe's theory and STCC formula. The mask pattern is the same as in Fig. 7. In the case of STCC formula we use SOCS model with 100 eigen modes for  $TCC$ , and 20 eigen modes for  $TCC_x$  and  $TCC_y$ . The difference between the image intensities calculated by the two formulas is small, less than 0.3%.

STCC formula reduces the computation time. The computation time of image intensity integration by Abbe's theory is 10 s for 512X512 points. While the computation by STCC formula takes only 0.07 s excluding the time for the eigen value decomposition by SOCS model.

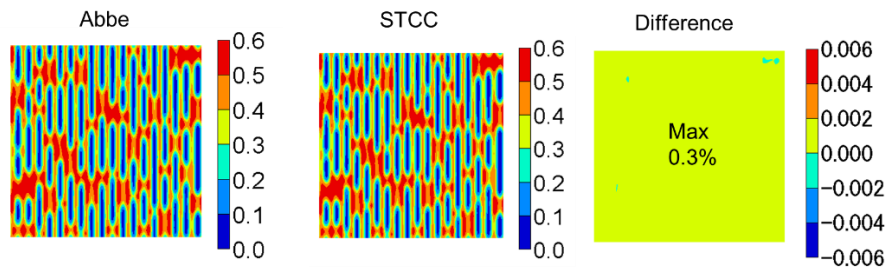


Fig. 8 Image intensities calculated by Abbe's theory and STCC formula.



Training data preparation	Training	Prediction
EM simulation	~2 days X12	M3D parameter prediction 0.05 s
3D waveguide 50 min/data → Weakly guiding 10 min/data	M3D parameters: Re $a_0$ , Re $a_x$ , Re $a_y$ Im $a_0$ , Im $a_x$ , Im $a_y$ for both Ax and Ay polarizations	Image intensity integration Abbe 10 s → STCC 0.07 s
2,000 data ~2 weeks		Total ~0.1 s
X400 data augmentation = 800,000 training data ~6 h		

Fig. 9 Run time of CNN data preparation, training, and prediction for 512 nm X 512 nm area.

## 5. SUMMARY

Figure 9 shows the estimation of the runtime for CNN data preparation, training, and prediction. Weakly guiding approximation reduces the time of EM simulation by a factor of 5, from 50 min to 10 min. STCC formula reduces the time of the image intensity integration by a factor of 140, from 10 s to 0.07 s. The total time of the image intensity prediction for 512 nm X 512 nm area on wafer (usable area: 200 nm X 200 nm) is ~0.1 s.

In this work we accelerated the EUV lithography simulation based on the CNN model. A remaining big issue is the accuracy of the CNN.<sup>15</sup> The accuracy depends on the quality and quantity of the training data. We hope that large-scale training mask data will improve the accuracy of the CNN.

## REFERENCES

- [1] V. Philipsen, "Mask is key to unlock full EUV potential," Proc. SPIE 11609(2021).
- [2] A. Erdmann, P. Evanschitzky, G. Bottiglieri, E. Setten and T. Fliervoet, "3D mask effects in high NA EUV imaging," Proc. SPIE 10957, 109570Z (2019).
- [3] A. Wong, "TEMPEST users' guide," UCB/ERL M94/64 (1994).
- [4] M.G. Moharam and T.K. Gaylord, "Rigorous coupled-wave analysis of planar-grating diffraction," J. Opt. Soc. Am. 71(1981) 811.
- [5] K.D. Lucas, H. Tanabe and A.J. Strojwas, "Efficient and rigorous three-dimensional model for optical lithography simulation," J. Opt. Soc. Am. A 13(1996)2187.
- [6] K. Adam and A. R. Neureuther, "Simplified models for edge transitions in rigorous mask modeling," Proc. SPIE 4346 (2001)331.
- [7] A. Erdmann, C. Kalus, T. Schmoeller and A. Wolter, "Efficient simulation of light from 3-dimensional EUV-masks using field decomposition techniques," Proc. SPIE 5037 (2003)482.
- [8] P. Liu, Y. Cao, L. Chen, G. Chen, M. Feng, J. Jiang, H. Liu, S. Suh, S.W. Lee and S. Lee, "Fast and accurate 3D mask model for full-chip OPC and verification," Proc. SPIE 6520 (2007)65200R.
- [9] J. Word, C. Zuniga, M. Lam, M. Habib, K. Adam and M. Oliver, "OPC modeling and correction solutions for EUV lithography," Proc. SPIE 8166 (2011)81660Q.
- [10] V. Domnenko, B. Kuechler, W. Hoppe, J. Preuninger, U. Klostermann, W. Demmerle, M. Bohn, D. Krueger, R. Ryoung, H. Kim and L.E. Tan, "EUV computational lithography using accelerated topographic mask simulation," Proc. SPIE 10962 (2019)169620O.
- [11] P. Liu, X. Xie, W. Liu and K. Gronlud, "Fast 3D thick mask model for full-chip EUVL simulations," Proc. SPIE 8679 (2013)86790W.
- [12] L. Zschiedrich, S. Burger, A. Schaedle and F. Schmidt, "Rigorous finite-element domain decomposition method for electromagnetic near field simulations," SPIE 6924 (2008)692450.
- [13] H. Tanabe, S. Sato and A. Takahashi, "Fast EUV lithography simulation using convolutional neural network," J. Micro/Nanopattern. Mater. Metrol. 20, 041202 (2021).

- [14] H. Tanabe and A. Takahashi, "Data augmentation in extreme ultraviolet lithography simulation using convolutional neural network," *J. Micro/Nanopattern. Mater. Metrol.* 21, 041602 (2022).
- [15] H. Tanabe, A. Jinguji and A. Takahashi, "Evaluation of convolutional neural network for fast extreme violet lithography simulation using 3nm node mask patterns," *J. Micro/Nanopattern. Mater. Metrol.* 22, 024201 (2023).
- [16] M. Born and E. Wolf, "Principles of Optics," 7th Ed. 1999.
- [17] A. Wong, "Resolution enhancement techniques in optical lithography," SPIE Press (2001).
- [18] H. Tanabe, "Modeling of optical images in resist by vector potentials," *Proc. SPIE* 1674 (1992)637.
- [19] D. Gloge, "Weakly guiding fibers," *Applied Optics* 10, 2252 (1971).
- [20] M. Yeung, "Modeling high numerical aperture optical lithography," *Proc. SPIE* 922 (1988)149.
- [21] N.B. Cobb, "Fast optical and process proximity correction algorithms for integrated circuit manufacturing," Ph.D. dissertation (University of California, Berkeley, 1998).